

Civil Engineering Journal

(E-ISSN: 2476-3055; ISSN: 2676-6957)

Vol. 11, No. 10, October, 2025



Passive Earth Pressure Analysis for Unsaturated Soils on Retaining Walls Incorporating Arching Effect

Ding-Jian Wang ^{1, 2}, Zhi-Qiang Fan ³, Qian-Yun Wang ^{1, 2}, Tao Wen ⁴, Ya-Hui Zhang ²

¹ Institute of Engineering Disaster Prevention and Mitigation, Hubei University of Education, Wuhan, 430205, China.

² Faculty of Engineering, China University of Geosciences, Wuhan 430074, Hubei, China.

³ PowerChina Huadong Engineering Corporation Limited, Hangzhou 310014, China.

⁴ School of Geosciences, International Cooperation Center for Mountain Multi-Disasters Prevention and Engineering Safety, Yangtze University, Wuhan, 430100, China.

Received 10 July 2025; Revised 21 September 2025; Accepted 29 September 2025; Published 01 October 2025

Abstract

Retaining structures in geological and geotechnical engineering are often embedded in unsaturated soil strata. Conventional methods for calculating earth pressure in unsaturated soils typically ignore the rotation of principal stresses in the backfill, a phenomenonknown as the soil arching effect. This study presents a novel analytical framework for determining the passive earth pressure in unsaturated soils that explicitly incorporates this arching effect. The proposed model accounts for both principal stress rotation and the hydro-mechanical coupling between matric suction and soil stress under groundwater influence. Based on the shear strength criterion for unsaturated soils, the model assumes a circular-arc trajectory for the rotating major principal stress, and hydrostatic seepage with matric suction distributed linearly with depth. Using a coordinate axis translation technique, quantitative relationships among lateral earth pressure, interlayer shear stress, and vertical stress are established. The force equilibrium equations for a horizontal differential soil element are then solved to derive closed-form expressions for the passive earth pressure distribution and resultant force. Validation against physical model tests and numerical simulations confirms the model's accuracy and demonstrates its superiority over the extended Rankine theory, which systematically underestimates passive resistance. Parametric studies highlight the influences of groundwater depth, initial matric suction, and soil strength parameters. The proposed framework offers a more realistic and mechanically sound basis for the design of retaining structures in unsaturated soil environments.

Keywords: Passive Earth Pressure; Unsaturated Soil; Soil Arching Effect; Matric Suction; Retaining Wall.

1. Introduction

The accurate estimation of earth pressure is fundamental to the design and analysis of retaining structures. Classical theories by Rankine and Coulomb provide a foundational framework, but their applicability is inherently limited to traditional saturated soil conditions. In reality, near-surface soils are often unsaturated, a condition characterized by the presence of matric suction [1]. This suction enhances soil strength by increasing effective stress, thereby altering the earth pressure distribution behind retaining walls [2]. Ignoring unsaturated conditions in conventional design can lead to non-conservative estimates, particularly for passive resistance, with potential implications for the safety and economy of geotechnical infrastructure [3].

^{*} Corresponding author: wangqianyun@cug.edu.cn





© 2025 by the authors. Licensee C.E.J, Tehran, Iran. This article is an open access article distributed under the terms and conditions of the Creative Commons Attribution (CC-BY) license (http://creativecommons.org/licenses/by/4.0/).

Significant research efforts have been devoted to extending earth pressure theory to unsaturated soils. The foundational work began with the shear strength criterion for unsaturated soils proposed by Fredlund & Rahardjo, which was subsequently integrated into the Rankine earth pressure framework [4]. Lu & Likos further advanced this by incorporating the effective stress principle for unsaturated soils, establishing an extended Rankine theory [5]. Subsequent studies have employed diverse methodologies, including slip-line theory [6], limit equilibrium methods with planar failure surfaces [7], and upper-bound limit analysis for complex scenarios such as rainfall infiltration [8]. Recent contributions continue to refine these models, accounting for transient seepage [9, 10], coupled hydromechanical processes [11], three-dimensional failure mechanisms [12], and layered soil backfill [13]. Collectively, these studies underscore the critical influence of matric suction and hydraulic conditions on lateral earth pressures.

Despite these advancements, a pervasive simplification in most existing unsaturated earth pressure models is the neglect of principal stress rotation caused by relative soil-wall displacement—a phenomenon known as the soil arching effect [14]. In conventional saturated soil mechanics, the profound influence of arching on earth pressure redistribution is well-recognized. Numerous physical model tests and in-situ monitoring programs have demonstrated that arching leads to a characteristic nonlinear stress distribution, contrasting sharply with the linear profiles predicted by classical theory [15-17]. Models incorporating arching, often by assuming a circular or catenary trajectory for the principal stresses, have consistently provided more accurate predictions for saturated backfills [18-20].

However, the interaction between matric suction and the soil arching effect remains rarely explored [3]. The assumption of uniform suction or the omission of stress rotation in current unsaturated models represents a significant oversimplification. This gap is particularly critical under passive loading conditions, where large displacements and pronounced arching effects are expected [21]. The coupling between the hydro-mechanical behavior induced by suction and the mechanical stress redistribution due to arching is likely to fundamentally control the resultant earth pressure. Nevertheless, a theoretical framework capable of capturing this synergy is currently lacking.

To address the aforementioned research gap, this paper develops a novel analytical model for passive earth pressure in unsaturated soils that explicitly incorporates the soil arching effect. The model is established based on the shear strength criterion for unsaturated soils and postulates a circular-arc trajectory for the rotating major principal stress. A coordinate translation technique is employed to derive stress transformation relationships, leading to the formulation and solution of differential equilibrium equations. The specific objectives of this study are: (1) to establish a theoretical framework that accounts for a hydrostatic, linearly varying matric suction profile, (2) to model the principal stress rotation using a circular arc and derive the corresponding stress relationships, and (3) to formulate closed-form solutions for the passive earth pressure distribution and resultant force.

The proposed model is validated against physical model tests and numerical simulations. A comprehensive parametric study is then conducted to elucidate the influences of key factors, including groundwater level, initial matric suction, and soil shear strength parameters. The findings provide a more realistic and mechanically rigorous approach for evaluating passive earth pressure in unsaturated soil-retaining wall systems.

2. Methodology

2.1. Fundamental Analysis Model

The fundamental physical model for calculating the earth pressure exerted by unsaturated soil on a retaining wall is illustrated in Figure 1. The soil behind the wall is divided into an unsaturated zone and a saturated zone, separated by the groundwater table (GWT). Extensive research shows that the specific distribution of matric suction depends critically on the soil's transient seepage state [1, 2, 22, 23]. Under hydrostatic conditions (i.e., no infiltration or evaporation), matric suction decreases with depth in the unsaturated zone, reaching its maximum at the ground surface and approaching zero at the GWT. Matric suction decreases during surface water infiltration and increases during evaporation or desiccation. This paper assumes a hydrostatic condition with the GWT located below the base of the retaining wall, ensuring unsaturated conditions at the wall toe. Under the idealized hydrostatic condition, matric suction follows a linear distribution with depth [2], described by:

$$s(z) = s_0 \left(1 - \frac{z}{h_W} \right) \tag{1}$$

where s(z) is the matric suction-the difference between pore air pressure (u_a) and pore water pressure (u_w) , at depth z below the ground surface, s_0 is the initial matric suction at the ground surface (z=0), and h_w is the depth to the GWT. Below the GWT $(z>h_w)$, matric suction is zero, and pore-water pressure is positive.

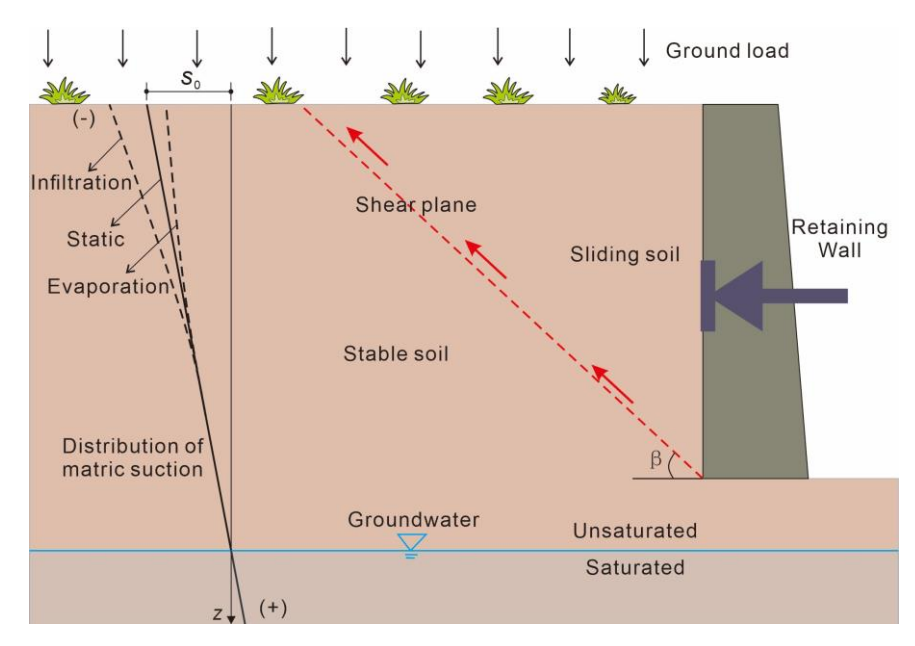


Figure 1. Schematic state of unsaturated soil behind the wall under passive force

When a retaining wall translates towards the backfill, the soil progressively transitions into a passive state to resist wall movement. As wall displacement increases, the soil ultimately undergoes shear failure. At the failure surface, the soil reaches a state of limit equilibrium, satisfying the unsaturated soil shear strength theory proposed by Lu and Likos [5]. This theory extends the classical Mohr-Coulomb criterion by incorporating the effective stress principle for unsaturated soils, expressed as:

$$\tau_f = (\sigma_f + \chi s) \tan \varphi' + c' \tag{2}$$

where τ_f and σ_f are the shear stress and net normal stress on the failure plane, respectively; φ' and ε' are the effective internal friction angle and effective cohesion of the soil, respectively; s is the matric suction; χ is the effective stress parameter, a dimensionless quantity ranging from 0 (dry) to 1 (saturation) that quantifies the contribution of suction to shear strength. Based on experimental and theoretical research by Van Genuchten [24] and Vanapalli & Fredlund [25], χ can be empirically related to the soil-water characteristic curve using an empirical formula often expressed in terms of the normalized degree of saturation:

$$\chi = \frac{\theta - \theta_r}{\theta_s - \theta_r} = \left[\frac{1}{1 + (\alpha s)^n} \right]^{1 - 1/n} \tag{3}$$

where θ , θ_s and θ_r represent the volumetric water contents of the soil in its natural, saturated, and residual states, respectively; α and n are SWCC fitting parameters.

Additionally, the analysis model incorporates the following simplifying assumptions to render the problem tractable while capturing the essential physics:

- The soil failure surface is planar, passing through the wall toe and inclined at an angle $\beta = \pi/4 \varphi'/2$ to the horizontal. This is consistent with the kinematic assumption of Rankine earth pressure theory for passive conditions [5].
- The soil above the GWT is homogeneous and isotropic, characterized by a uniform natural unit weight γ , effective cohesion c', and effective internal friction angle φ' . Soil properties below the GWT correspond to the saturated state.
- The retaining wall is rigid and translates horizontally without deformation or rotation. Its back face is vertical and perfectly rough (frictional).
- The ground surface is subjected to a uniform surcharge load of intensity p, representing overburden or traffic loading.
- The air phase is continuous and at atmospheric pressure $(u_a = 0)$, a reasonable assumption for near-surface unsaturated soils.

2.2. Stress State Analysis for Unsaturated Soil Behind the Wall

When a retaining wall remains stationary relative to the adjacent soil, the soil is in an at-rest state (K_0 condition), characterized by a vertically oriented major principal stress (σ_1) and a horizontally oriented minor principal stress (σ_3). As the wall translates towards the soil mass, relative displacement induces shear interaction along the soil-wall interface. This interaction progressively rotates the major and minor principal stresses within the soil. The magnitude of the rotation increases with wall displacement until the soil reaches a state of limit equilibrium, as conceptually illustrated in Figure 2. This phenomenon, known as the soil arching effect, arises from differential movement and stress redistribution within the confined soil mass. The soil arching effect has been observed in numerous physical model tests [26-29]. Consequently, many researchers have developed earth pressure estimation models for retaining structures that incorporate the arching effect [30-33]. However, these models primarily address conventional earth pressure calculations for saturated soils and do not explicitly account for the unique characteristics of unsaturated soils, particularly the influence of spatially varying matric suction on shear strength and its interaction with principal stress rotation.

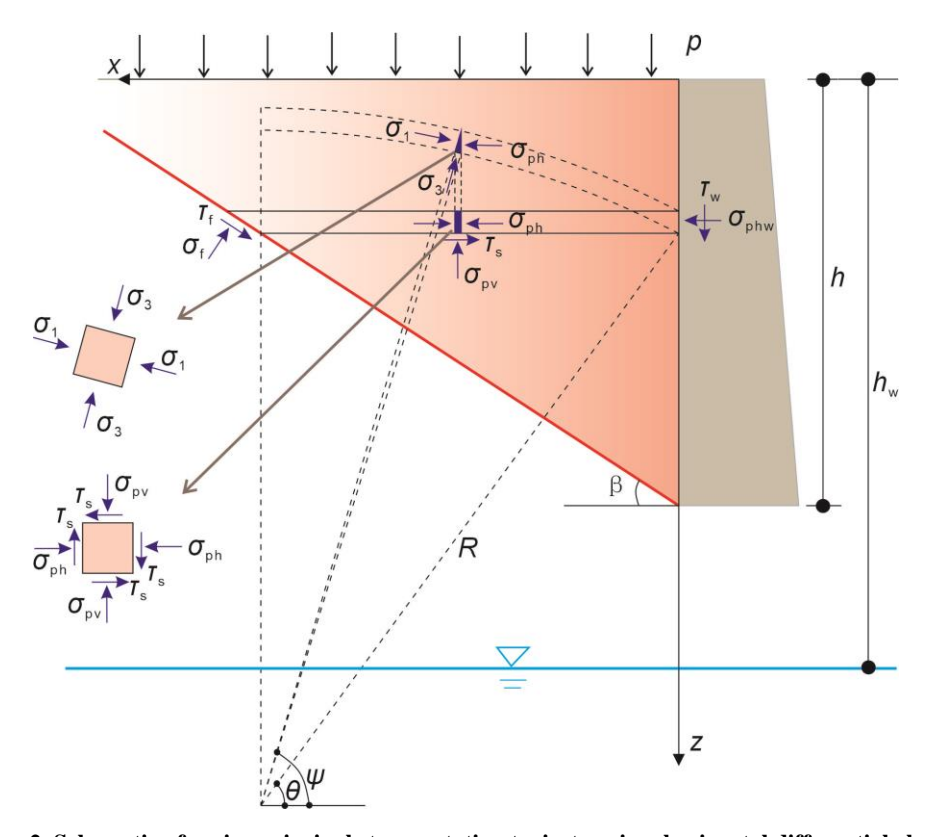


Figure 2. Schematic of major principal stress rotation trajectory in a horizontal differential element

Building upon previous research, this paper proposes a new analytical model applicable to passive earth pressure calculation for unsaturated soils, explicitly incorporating the arching effect. Consider a horizontal differential element of soil located at depth z behind the wall, as shown in Figure 2. Within this element, the trajectory of the rotated major principal stress is assumed to form a circular arc of radius R. This geometric assumption, widely adopted in traditional arching-based earth pressure models [30, 34-36], facilitates the mathematical description of principal stress rotation. Let ψ denote the angle between the minor principal stress and the horizontal at any position within the element. At the shear failure plane of the soil, compatibility requires the minor principal stress to be oriented vertically (i.e., $\psi = 90^{\circ}$). At the wall-soil interface, the angle between the minor principal stress and the horizontal is defined as θ , which is a function of the wall-soil interface friction angle δ .

The stress state of the horizontal differential element can be described by the Mohr circle in the (σ, τ) coordinate system as shown in Figure 3. The following geometric relationship is obtained:

$$\begin{cases} \frac{\sigma_{\rm ph}}{\sigma_1} = \sin^2 \psi + \frac{\sigma_3}{\sigma_1} \cos^2 \psi \\ \frac{\sigma_{\rm pv}}{\sigma_1} = \cos^2 \psi + \frac{\sigma_3}{\sigma_1} \sin^2 \psi \\ \frac{\tau_s}{\sigma_1} = (1 - \frac{\sigma_3}{\sigma_1}) \sin \psi \cos \psi \end{cases} \tag{4}$$

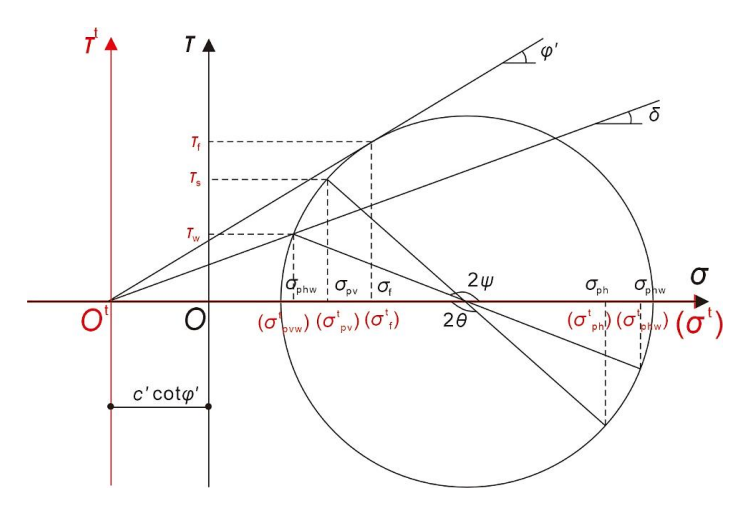


Figure 3. Schematic of coordinate axis translation and Mohr stress circle for the soil

Equation 4 relates the normal and shear stresses at a certain position within the horizontal differential element to its position. However, the results calculated from this equation are variable, as the ratio σ_3/σ_1 changes with ψ and is also dependent on both c' and φ' . To address this analytical challenge, the coordinate axis translation technique is employed. The vertical axis of the coordinate system (τ) is shifted leftward by a magnitude c' cot φ' , resulting in a new coordinate system (σ^t , τ^t), indicated by the red axes in Figure 3. In the transformed coordinate system, the Mohr-Coulomb failure envelope passes through the origin (O^t). The geometric relationship within this new system yields a simplified expression for the principal stress ratio:

$$\lambda = \frac{\sigma_3^t}{\sigma_1^t} = \frac{1 - \sin \varphi'}{1 + \sin \varphi'} \tag{5}$$

Equation 5 shows that in the new coordinate system (σ^t , τ^t), the ratio of minor to major principal stress is constant, depending only on the effective internal friction angle. Therefore, Equation 4 in the transformed coordinate system can be expressed as:

$$\begin{cases} \frac{\sigma_{\rm ph}^t}{\sigma_1^t} = \sin^2 \psi + \lambda \cos^2 \psi \\ \frac{\sigma_{\rm pv}^t}{\sigma_1^t} = \cos^2 \psi + \lambda \sin^2 \psi \\ \frac{\tau_s}{\sigma_1^t} = (1 - \lambda) \sin \psi \cos \psi \end{cases}$$
 (6)

where the results are univariate function about ψ .

At the wall-soil interface, the stress state must satisfy the interface failure criterion, represented by a straight line inclined at angle δ (the wall-soil interface friction angle) to the σ^t axis. The geometric relationship between the envelope and the Mohr circle is established as:

$$\tau_{w} = \frac{1}{2}(\sigma_{1}^{t} - \sigma_{3}^{t})\sin(\pi - 2\theta) = \left[\frac{1}{2}(\sigma_{1}^{t} + \sigma_{3}^{t}) + \frac{1}{2}(\sigma_{1}^{t} - \sigma_{3}^{t})\cos(\pi - 2\theta)\right]\tan\delta\tag{7}$$

where τ_w are is shear stress at the wall-soil interface. Solving Equation 7 in conjunction with the Mohr circle geometry gives the value of the angle θ :

$$\theta = \arctan \frac{1 - \lambda + \sqrt{(1 - \lambda)^2 - 4\lambda \tan^2 \delta}}{2 \tan \delta}$$
 (8)

In the transformed coordinate system, the total vertical force (V^t) acting on the horizontal differential element of width $R\cos\theta$ is:

$$V^{t} = \int_{\theta}^{\pi/2} \sigma_{1}^{t} (\cos^{2} \psi + \lambda \sin^{2} \psi) R \sin \psi \, d\psi = \sigma_{1}^{t} R \left[\frac{1}{2} (1 - \lambda) \cos^{3} + \lambda \cos \theta \right] \tag{9}$$

The average transformed vertical stress $(\bar{\sigma}_{pv}^t)$ on the element is thus:

$$\bar{\sigma}_{pv}^{t} = \frac{v^{t}}{R\cos\theta} = \sigma_{1}^{t} \left[\frac{1}{3} (1 - \lambda) \cos^{2}\theta + \lambda \right]$$
 (10)

Define the lateral earth pressure coefficient (K_{pw}) in the transformed coordinate system as the ratio of the transformed lateral pressure stress on the wall (σ_{phw}^t) to the average transformed vertical stress:

$$K_{\rm pw} = \frac{\sigma_{\rm phw}^t}{\sigma_{\rm nv}^t} = \frac{3(\sin^2\theta + \lambda\cos^2\theta)}{(1-\lambda)\cos^2\theta + 3\lambda} \tag{11}$$

The total shear force (T) acting on the top surface of the horizontal differential element (arising from shear stresses τ_s on vertical planes within the soil mass due to arching) is:

$$T = \int_{\theta}^{\pi/2} \sigma_1^t (1 - \lambda) \sin \psi \cos \psi \cdot R \sin \psi \, d\psi = \frac{1}{3} \sigma_1^t R (1 - \lambda) (1 - \sin^3 \theta) \tag{12}$$

Correspondingly, the average interlayer shear stress $(\bar{\tau}_s)$ is:

$$\bar{\tau}_S = \frac{T}{R\cos\theta} = \frac{\sigma_1^t(1-\lambda)(1-\sin^3\theta)}{3\cos\theta}$$
 (13)

Define the interlayer shear coefficient (K_{ps}) in the transformed coordinate system as the ratio of the average transformed interlayer shear stress to the average transformed vertical stress:

$$K_{\rm ps} = \frac{\bar{\tau}_s}{\bar{\sigma}_{\rm pv}^t} = \frac{(1-\lambda)(1-\sin^3\theta)}{(1-\lambda)\cos^3 + 3\lambda\cos\theta} \tag{14}$$

From Equations 11 and 14, it is evident that K_{pw} and K_{ps} are independent of the horizontal differential element width and its depth. They depend solely on λ and θ , which are, in turn, functions of φ' and δ . Therefore, K_{pw} and K_{ps} are ultimately determined by the frictional properties of the backfill soil and wall-soil interface, reflecting the fundamental frictional nature of the arching mechanism within the transformed stress space. These coefficients are essential for establishing the differential equilibrium equations in the subsequent section.

2.3. Mechanical Equilibrium Equations for Differential Soil Element

Consider the horizontal differential element of soil behind the wall shown in Figure 2. Its geometric dimensions and force diagram are illustrated in Figure 4. The element has a differential height dz, located at depth z below the ground surface. The width of the element is $(h-z) \cot \beta$. Force equilibrium in both horizontal (x) and vertical (z) directions must be satisfied:

$$\begin{cases}
\sigma_{\text{phw}}dz + \bar{\tau}_s(H - z)\cot\beta - (\bar{\tau}_s + d\bar{\tau}_s)(H - z - dz)\cot\beta - \sigma_f dz - \tau_f \cot\beta dz = 0 \\
(\bar{\sigma}_{\text{pv}} + d\bar{\sigma}_{\text{pv}})(H - z - dz)\cot\beta - \bar{\sigma}_{\text{pv}}(H - z)\cot\beta - \tau_w dz + \sigma_f \cot\beta dz - \tau_f dz - \gamma(H - z)\cot\beta dz = 0
\end{cases}$$
(15)

where the variables can be further calculated or related as follows:

$$dG = \gamma (H - z) \cot \beta \, dz \tag{16}$$

$$\sigma_{phw} = \sigma^t_{phw} - c_\chi \cot \varphi' = K_{pw} \bar{\sigma}^t_{pv} - c_\chi \cot \varphi' = K_{pw} (\bar{\sigma}_{pv} + c_\chi \cot \varphi') - c_\chi \cot \varphi' = K_{pw} \bar{\sigma}_{pv} + c_\chi (K_{pw} - 1) \cot \varphi' \qquad (17)$$

$$\bar{\tau}_{S} = K_{DS}\bar{\sigma}_{DV}^{t} = K_{DS}\bar{\sigma}_{DV} + c_{\gamma}K_{DS}\cot\varphi' \tag{18}$$

$$\tau_{w} = \bar{\sigma}_{phw}^{t} \tan \delta = \bar{\sigma}_{pv} K_{pw} \tan \delta + c_{x} K_{pw} \cot \varphi ' \tan \delta$$
 (19)

$$c_{\gamma} = c' + \chi s \tan \varphi$$
 (20)

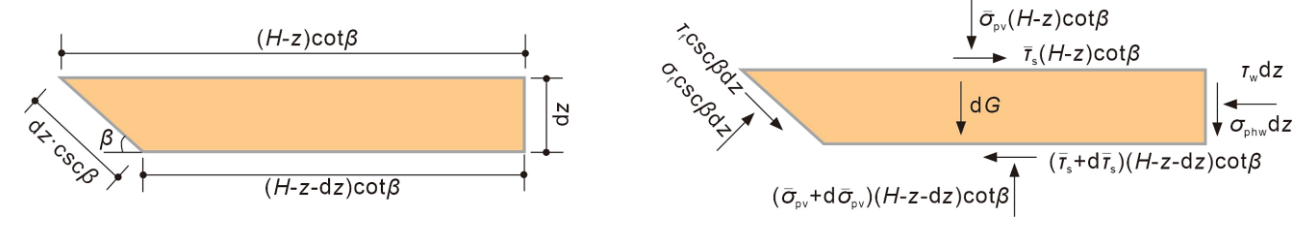


Figure 4. Geometric dimensions and force analysis of a horizontal differential element

Equations 17 to 19 establish the relationships among the stress components in the original coordinate system through coefficients K_{pw} , K_{ps} and coordinate translation. Substituting Equations 16 to 20 into Equation 15, and solving simultaneously yields the following first-order non-homogeneous linear differential equation for $\bar{\sigma}_{pv}$:

$$\frac{d\bar{\sigma}_{pv}}{dz} + \frac{A\bar{\sigma}_{pv}}{H-z} = \frac{C}{H-z} + B \tag{21}$$

where A, B and C are constants, and their specific expressions are as follows:

$$A = \frac{\tan(\beta + \varphi') + K_{\text{pw}} \tan(\beta + \varphi') \tan\beta \tan\delta - K_{\text{pw}} \tan\beta - K_{\text{ps}}}{K_{\text{ps}} - \tan(\beta + \varphi')}$$
(22)

$$B = \frac{\gamma \tan(\beta + \varphi')}{\tan(\beta + \varphi') - K_{ps}} + \frac{\chi s_0 D \tan \varphi'}{\Box_w}$$
 (23)

$$C = c' + \chi s_0 \left(1 - \frac{\Box}{\Box_{tr}} \right) \tan \varphi ' \tag{24}$$

$$D = \frac{\left[K_{\text{pw}} - K_{\text{pw}} \tan(\beta + \varphi') \tan\delta - 1\right] \tan\beta \cot \varphi' + K_{\text{ps}} \cot \varphi' - \tan(\beta + \varphi') \tan\beta - 1}{K_{\text{ps}} - \tan(\beta + \varphi')}$$
(25)

Equation 21 establishes the fundamental equilibrium equation for the horizontal differential element of the soil mass behind the wall. By solving this equation, an explicit expression for the passive earth pressure can be obtained.

2.4. Summary of Methodology

As outlined above, a calculation model for passive earth pressure that accounts for the soil arching effect has been established. The basic framework of this model is depicted in the flowchart shown in Figure 5. To summarize, the derivation follows these steps: First, determine an appropriate strength criterion for unsaturated soil and a model for the distribution of matric suction. Subsequently, based on simplified assumptions, identify the failure surface of the soil behind the wall and construct a corresponding model for the horizontal differential element of the soil. Furthermore, consider the rotation of principal stresses to conduct an analysis of the stress state within the soil, and calculate the lateral earth pressure coefficient and the interlayer shear coefficient based on this analysis. Building on this foundation, and utilizing the aforementioned strength criterion and suction distribution model, establish the differential equation for the force equilibrium of the horizontal differential soil element. Finally, solve the differential equation and compute the passive earth pressure.

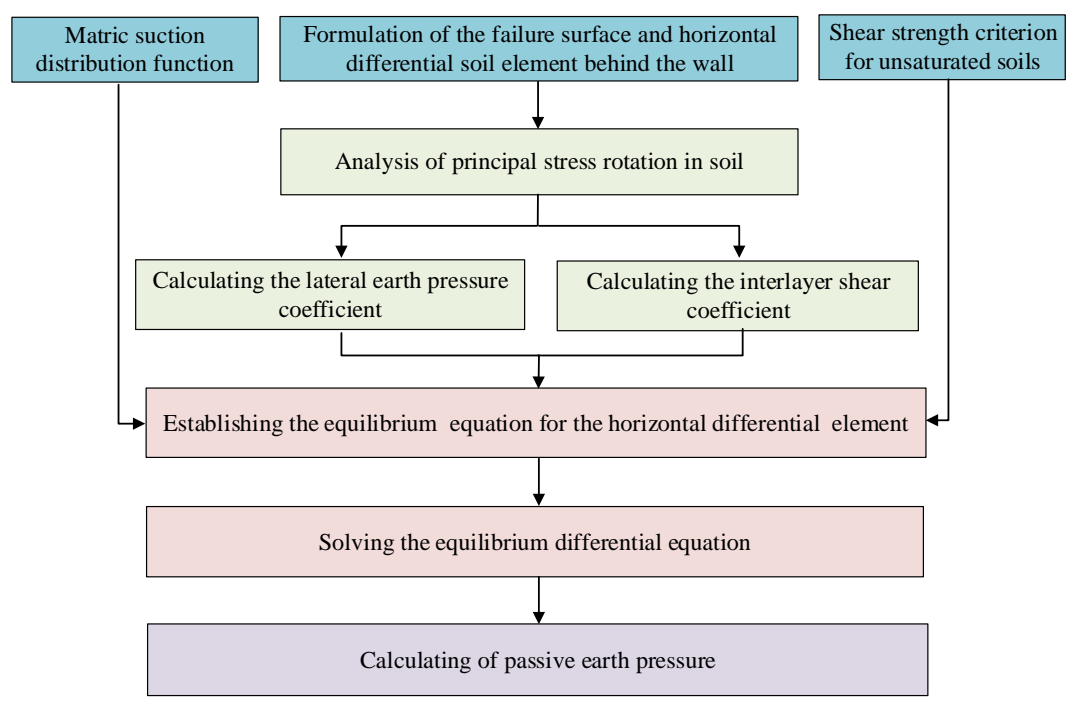


Figure 5. Flowchart of passive earth pressure analysis for unsaturated soils incorporating arching effect

3. Results

The explicit expression for the horizontal passive earth pressure can be obtained by solving Equation (21). Solving the equation requires an integration followed by applying the boundary condition at the ground surface (z=0), where the vertical stress equals the applied surcharge: $\bar{\sigma}_{pv}|z=0=p$. The solution yields the average vertical stress with depth:

$$\bar{\sigma}_{pv} = \frac{Bh}{A-1} \left[\left(1 - \frac{z}{h} \right) - \left(1 - \frac{z}{h} \right)^A \right] + \frac{c}{A} \left[1 - \left(1 - \frac{z}{h} \right)^A \right] + p \left(1 - \frac{z}{h} \right)^A$$
 (26)

Combining Equations 17 and 26, the distribution function for the horizontal passive earth pressure (σ_{phw}) for unsaturated soil is obtained:

$$\sigma_{\rm phw} = \frac{\kappa_{\rm pw}Bh}{A-1} \left[\left(1 - \frac{z}{h}\right) - \left(1 - \frac{z}{h}\right)^A \right] + \frac{\kappa_{\rm pw}C}{A} \left[1 - \left(1 - \frac{z}{h}\right)^A \right] + \kappa_{\rm pw}p \left(1 - \frac{z}{h}\right)^A + \left[c' + \chi s_0 \tan \varphi' \left(1 - \frac{z}{h_w}\right)\right] (\kappa_{\rm pw} - 1)\cot \varphi' \quad (27)$$

The calculation of passive earth pressure using Equation 27 can be carried out in three steps:

First, calculate the coefficients of the soil arching effect (K_{pw} and K_{ps}). These two coefficients are solely functions of the soil's effective friction angle (φ') and the wall-soil interface friction angle (δ). Engineers can directly compute them using Equations 11 and 14.

Second, calculate the coefficients of the earth pressure function (*A*, *B*, *C* and *D*). These coefficients are isolated from the earth pressure function to make its expression more intuitive and clear. They are calculated using Equations 22-25.

Finally, compute the passive earth pressure. After obtaining the coefficients of the earth pressure function, Equation 27 can be directly used to calculate the passive earth pressure, ultimately yielding the distribution profile of the passive earth pressure.

Integrating Equation 27 vertically over the wall height h gives the resultant force of horizontal passive earth pressure (E_p) :

$$E_p = \int_0^h \sigma_{\text{phw}} dz = \frac{K_{\text{pw}} h(Bh + 2C + 2p)}{2(A+1)} + (K_{\text{pw}} - 1)h \left[c' \cot \varphi' + \chi s_0 \left(1 - \frac{h}{2h_w} \right) \right]$$
 (28)

Equations 27 and 28 indicate that passive earth pressure depends critically on the physical parameters of the unsaturated soil (γ , c', φ' , SWCC parameters), the initial matric suction (s_0), the wall-soil friction angle (δ), the groundwater depeth (h_w), and the surcharge (p). Compared to unsaturated earth pressure models derived by conventional methods neglecting arching (e.g., extended Rankine theory), the proposed approach incorporates the effect of principal stress rotation behind the wall. The resulting passive earth pressure exhibits a characteristically nonlinear distribution with depth, reflecting the real stress state of the soil influenced by both suction and the arching effect. The equations simplify to the following special cases when specific parameters are modified:

- (1) Deep groundwater $(h_w \to \infty)$: The matric suction throughout the profile becomes constant, equal to the initial matric suction $(s = s_0)$. Equation 27 degenerates into a formula for calculating the passive earth pressure of unsaturated soil without considering the groundwater level.
- (2) Zero Initial Matric Suction ($s_0 = 0$): There is no matric suction on the soil profile, and Equation 27 degenerates into the conventional formula for calculating the passive earth pressure of soil without considering its unsaturated characteristics.
- (3) Zero Effective Cohesion (c'=0): Equation (27) degenerates into a calculation formula for passive earth pressure of non-cohesive soil.

4. Validation

4.1. Validation with Physical Model Test

To validate the proposed theoretical model, a comparative analysis is performed against the experimental results reported by Vo & Russell [6]. Their comprehensive series of physical model tests involved vertical retaining walls rotated about their toes towards a backfill of uniform unsaturated silty sand. During wall rotation, passive earth pressure developed progressively, accompanied by the formation of a plastic soil wedge. Six distinct tests were conducted, with each specimen compacted to an identical initial water content to maintain consistent initial matric suction (except Test 6). The physical models explicitly excluded wall-top surcharge (p = 0) and groundwater effects, implying constant matric suction ($s = s_0$). Results from Tests 4 and 5 in the developed passive failure states (medium dense sand, final wall rotation angle = 6.94°), are selected for validation.

It is important to note that as the wall movement mode was rotation about the toe rather than pure translation, the experimental data consistently indicated that soil strength was not fully mobilized in the lower portion of the wall. Below approximately two-thirds of the wall height (z/h > 2/3), the measured passive earth pressure decreased sharply, and the propagation rate of the observed plastic zone slowed significantly. Consequently, the present theoretical solution, which is derived on the basis of a translation-movement assumption, is considered primarily applicable for calculating passive earth pressure from the wall top down to 2h/3 depth (corresponding to the fully developed plastic zone). For the lower h/3 depth, the passive earth pressure is estimated to decrease linearly from the value calculated at 2h/3 to zero at the wall toe. This pragmatic approach is conceptually consistent with "Approach 2" proposed by Vo & Russell [6] for reconciling rotation test results with translation-based theories. The physical parameters of the backfill soil in Tests 4 and 5, required as model inputs, are summarized in Table 1.

Table 1. Parameters for physical model tests by Vo & Russell [6]

Test number	Test 4	Test 5		
Density description	Medium dense	Medium dense		
Water content (%)	5.5	4.5		
Rotation of wall (°)	6.94	6.94		
h (m)	0.5315	0.5365		
c' (kPa)	0	0		
φ (°)	40.7	40.7		
$\gamma (kN/m^3)$	17.1	17		
s (kPa)	27.9	59.5		
χ	0.219	0.194		

The horizontal earth pressure calculated using Equation 27 is compared with the measured test data in Figure 6. The results demonstrate that the proposed theoretical solution effectively captures the nonlinear characteristics of passive earth pressure. Within the upper 2h/3 depth, the solution agrees well with the experimental results. For the lower h/3 depth, where the soil remains in an elastic state without full strength mobilization, a linear reduction approach (depicted by the dashed line in the figure) also provides a good fit to the test data. The agreement between theoretical predictions and experimental measurements validates the effectiveness of the proposed solution. Although minor discrepancies exist, potential contributing factors include: (1) the rotation mode employed in the model tests, contrasting with the assumed translation mode; and (2) possible scale effects arising from the small size of the model tests, which may influence measurements.

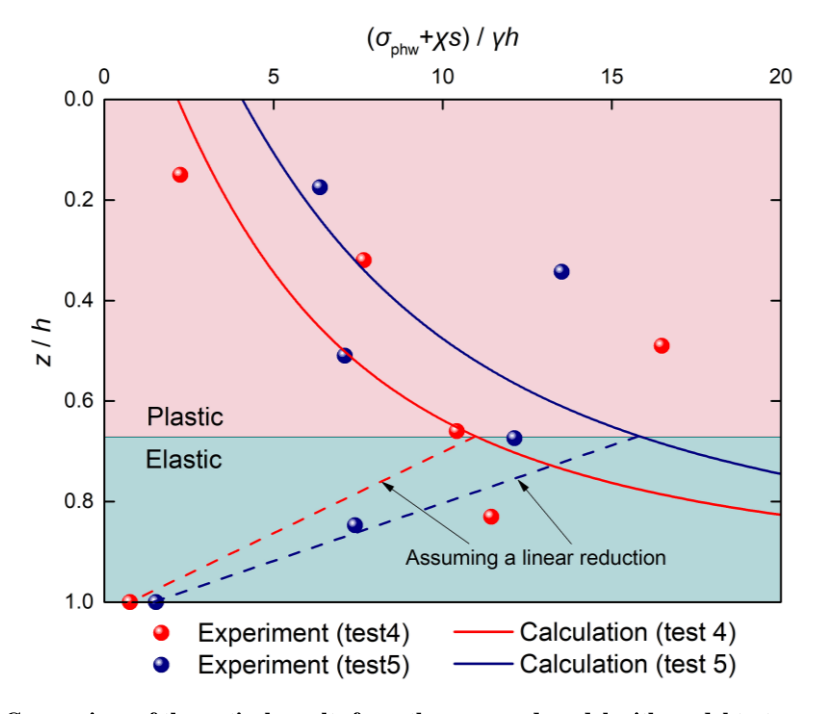


Figure 6. Comparison of theoretical results from the proposed model with model test measured data

4.2. Validation with Numerical Simulation

To further validate the proposed analytical model beyond physical model tests and provide an independent assessment of its performance, a numerical simulation was conducted using the Finite Difference Code FLAC.

A full-scale model of a rigid retaining wall with a height of 3 m, translating horizontally into the unsaturated backfill, was established. The soil parameters were consistent with those listed in Table 2 for the case study. The model mesh and boundary conditions are illustrated in Figure 7-a. Direct simulation of unsaturated soil hydromechanical coupling in FLAC is not standard. Therefore, an alternative approach was implemented via its built-in FISH scripting language. The contribution of matric suction to soil strength was represented by an apparent cohesion ($\chi stan\varphi'$) calculated for each soil element based on the theoretical linear suction profile and the effective stress parameter. The total cohesion assigned to each element was then updated to be the sum of the effective cohesion and the apparent cohesion, thereby effectively capturing the enhanced shear strength due to matric suction.

Table 2. Physical parameters for numerical study model

Parameter	α (kPa ⁻¹)	n	c' (kPa)	φ'(°)	$\gamma (kN/m^3)$	h (m)	$h_{\rm w}({\rm m})$	δ (°)	s ₀ (kPa)	p (kPa)
Value	0.02	4	15	30	18	3	5	15	100	10

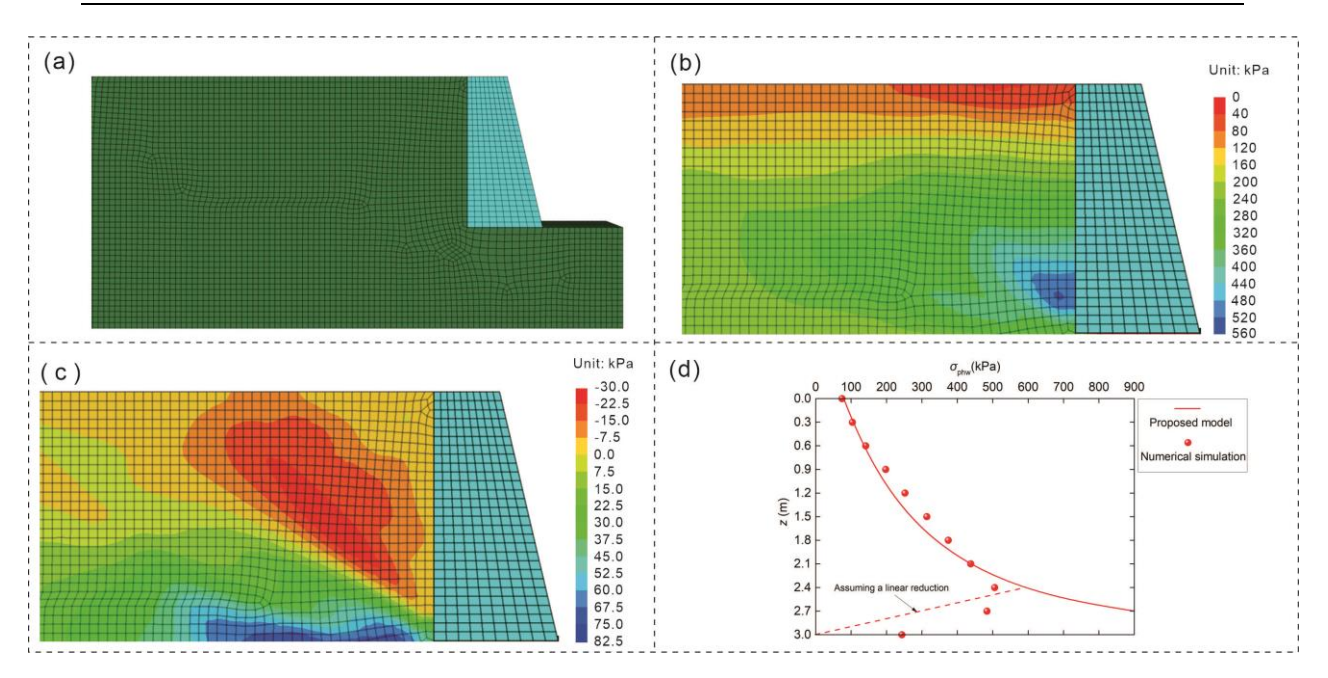


Figure 7. Numerical model and comparison with proposed analytical solution: (a) FLAC model; (b) Contours of horizontal normal stress at passive state; (c) Contours of shear stress at passive state; (d) Comparison of the proposed model results with numerical simulation data.

Figures 7-b and 7-c present the contours of horizontal normal stress and shear stress within the soil mass at the passive failure state, respectively. The development of a passive failure wedge and the nonlinear stress distribution behind the wall are clearly observed. The horizontal earth pressure profile monitored at the wall-soil interface is plotted against the prediction of the proposed analytical model in Figure 7-d.

The comparison reveals a high level of agreement. Within the upper 0.8h depth, the horizontal pressure from the numerical simulation increases nonlinearly with depth and aligns remarkably well with the theoretical curve. This close correspondence provides strong, independent confirmation of the proposed model's accuracy in the zone where soil arching is fully mobilized. Below the depth of 0.8h, the numerical results show a slight decrease in pressure, a phenomenon also noted in physical model tests involving wall rotation. In contrast, the analytical model, derived for a pure translational mode, predicts a continued increase. This discrepancy underscores that the soil near the wall toe may not be fully mobilized to a passive state under certain boundary conditions. Consequently, for practical design applications, applying a linear reduction to the theoretical pressure below a depth of 0.8h, as illustrated by the dashed line in Figure 7-d, is a justified and conservative approach.

In summary, the numerical simulation not only corroborates the predictive capability of the proposed model within the primary zone of interest but also clarifies its behavior near the wall base, thereby enhancing the overall confidence in the analytical solution.

5. Discussion

This section presents a case study to investigate the distinctions between the proposed analytical model and the extended Rankine theory. A parametric sensitivity analysis is subsequently conducted to assess the model's applicability. The case model is the same as the numerical simulation model in Section 4.2, and the physical parameters for the model are presented in Table 2. For the sensitivity analysis, the value of a single parameter from the table is systematically varied while holding others constant, and the consequent variations in the calculations are compared.

5.1. Comparison with Extended Rankine Theory

Lu & Likos [5] integrated the effective stress principle into classical Rankine earth pressure theory, resulting in the extended Rankine passive earth pressure formula:

$$\sigma_{\rm phw} = \gamma z \tan^2\left(\frac{\pi}{4} + \frac{\varphi'}{2}\right) + 2c'\tan\left(\frac{\pi}{4} + \frac{\varphi'}{2}\right) + 2\chi s \tan\varphi' \tan\left(\frac{\pi}{4} + \frac{\varphi'}{2}\right) \tag{29}$$

However, it is widely recognized that Rankine theory is strictly applicable only for smooth wall backs (δ =0), limiting its practical utility. In the present comparison study, the horizontal passive earth pressure and resultant force computed by the proposed model are compared with those predicted by the extended Rankine theory in Figure 8. Both axes are normalized to facilitate comparison. As Equation 27 does not converge when δ =0, calculations for δ/φ' ratios ranging from 0.001 to 1.0 are presented for comparison.

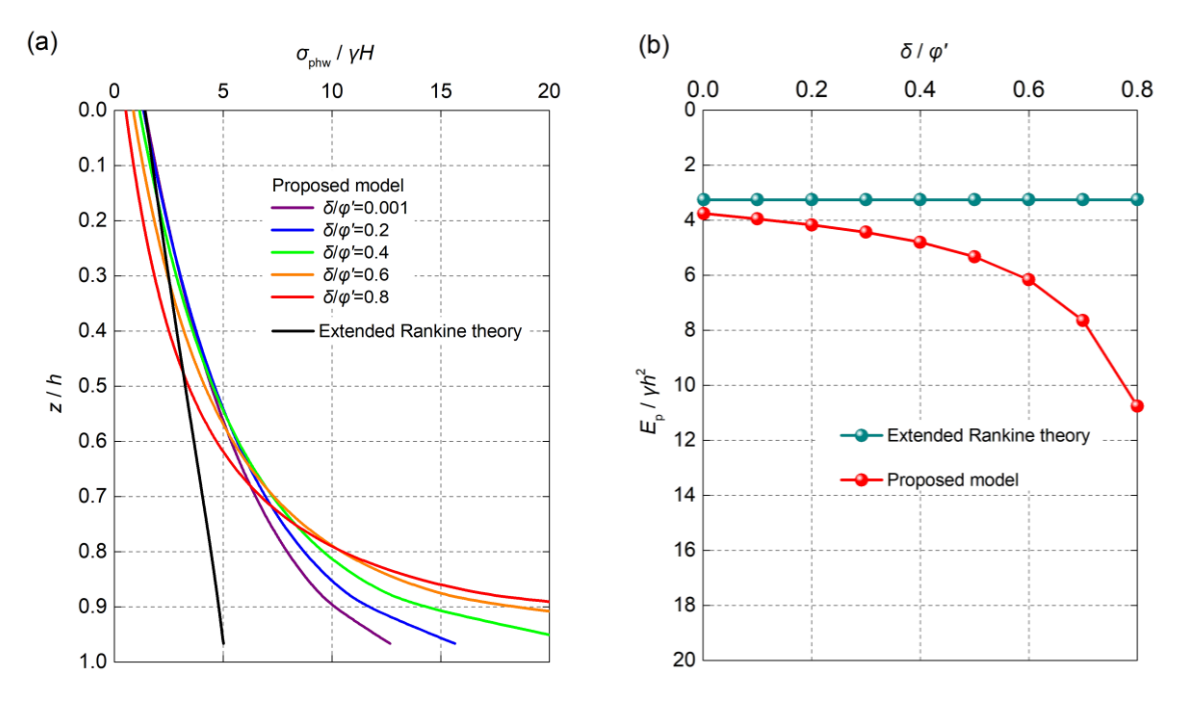


Figure 8. Comparison between proposed model and extended Rankine theory: (a) passive earth pressure distribution; (b) resultant force

Figure 8-a demonstrates that passive earth pressure increases with depth, with the curvature of the distribution curve also increasing, exhibiting an approximately exponential trend. In shallow region (z/h < 0.5), the horizontal passive pressure diminishes as δ/φ' increases. Conversely, in deeper region (z/h > 0.5), the pressure increases with increasing δ/φ' . Compared to the extended Rankine theory, the proposed model yields lower pressure near the surface and higher pressure at greater depths.

Figure 8-b reveals that the resultant force calculated by the extended Rankine theory is significantly smaller than that obtained from the proposed model. This outcome indicates that the extended Rankine theory substantially underestimates the magnitude of passive earth pressure. Furthermore, the Rankine resultant force exhibits no dependence on δ , which is physically unrealistic. In contrast, the resultant force predicted by the proposed model increases with increasing δ/φ' . Notably, the rate of increase is gradual for low δ/φ' values and accelerates at higher values. When δ/φ' exceeds 0.8, the resultant force increases drastically to unrealistic levels. Although this phenomenon has been reported in some literature utilizing arching theory for traditional soil passive pressure [37, 38], it warrants caution. Consequently, it is recommended that the proposed model be applied under the condition $\delta/\varphi' < 0.8$.

5.2. Parametric Study

This section examines the influences of four key parameters on horizontal passive earth pressure and resultant force: groundwater table depth (h_w) , initial matric suction at the ground surface (s_0) , effective internal friction angle (φ') , and effective cohesion (c').

Figure 9 illustrates the variation in horizontal passive earth pressure and resultant force with groundwater depth. Figure 9-a indicates that the passive pressures near the surface are similar across different $h_{\rm w}$ values. However, with increasing groundwater depth, the differences become more pronounced, with larger $h_{\rm w}$ values corresponding to higher passive pressures. Figure 9-b shows that when the GWT is shallow, the resultant force increases rapidly with increasing $h_{\rm w}$, although the rate of increase (indicated by the curve's slope) gradually diminishes. When $h_{\rm w}$ exceeds 10 m, the curve flattens considerably, and the resultant force increases very slowly, approaching a stable value. In practical engineering applications, close attention should be paid to scenarios involving a shallow GWT, as passive earth pressure is highly sensitive to water level fluctuations within this range.

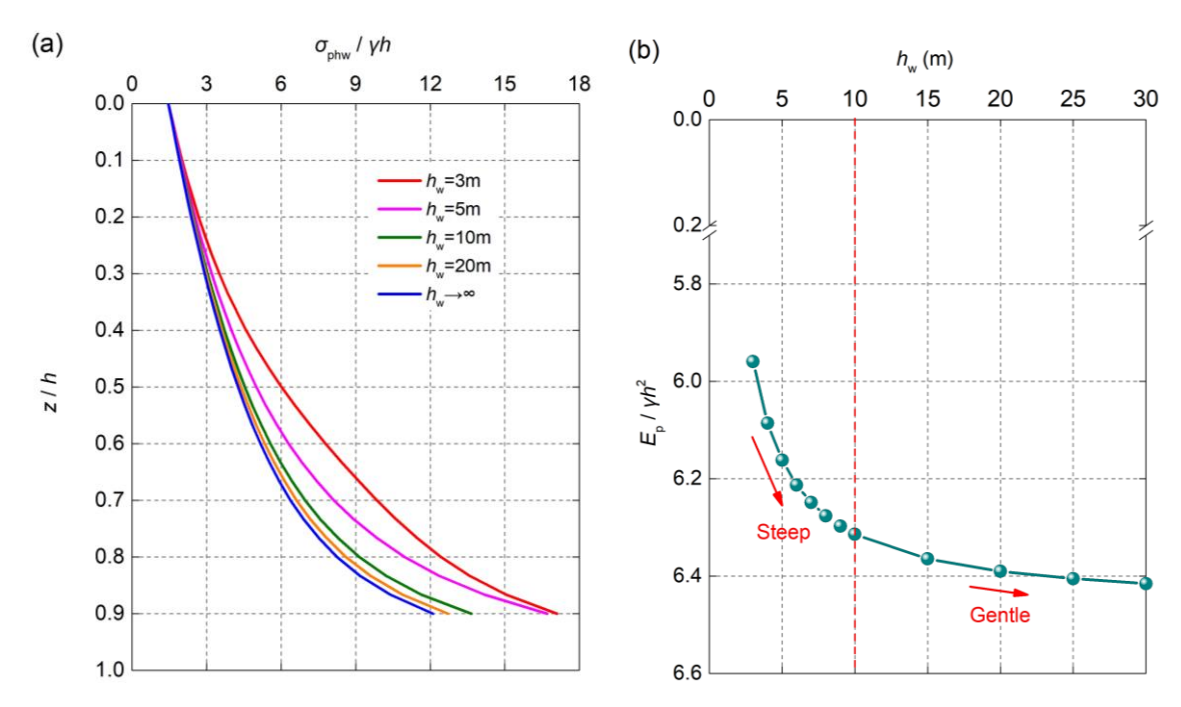


Figure 9. Influence of groundwater table depth on passive earth pressure: (a) distribution; (b) resultant force

Figure 10 depicts the effect of initial matric suction on horizontal passive earth pressure and resultant force. For s_0 values less than 50 kPa, passive earth pressure increases rapidly with increasing suction. When s_0 exceeds 50 kPa, passive earth pressure initially decreases rapidly and subsequently stabilizes. This behavior is counterintuitive: passive earth pressure does not attain its maximum value under conditions of either very high or very low suction, but rather at an intermediate state (50 kPa in this case study).

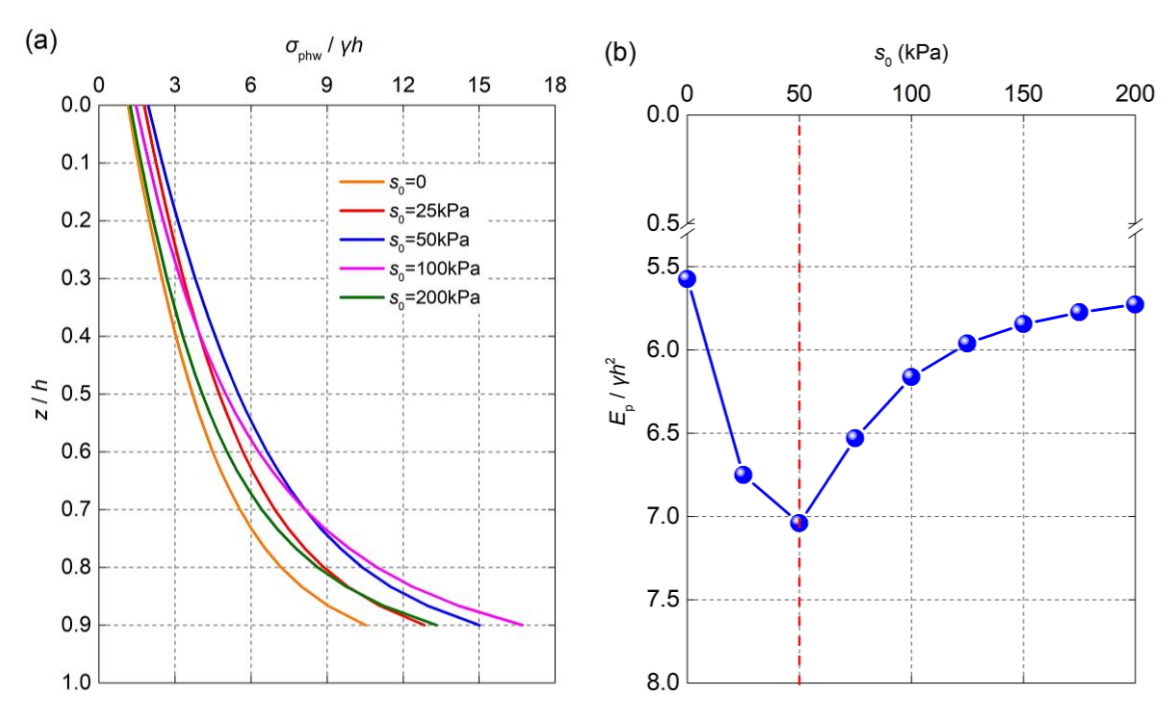


Figure 10. Influence of initial matric suction on passive earth pressure: (a) distribution; (b) resultant force

Figure 11 presents the variation of passive earth pressure and resultant force with the effective internal friction angle. Figure 11-a demonstrates that φ' significantly influences the shape of the earth pressure curve. At low φ' values, the pressure increases slowly with depth. Conversely, at high φ' values, it increases rapidly with depth. The variation pattern of the resultant force resembles that of the soil pressure. When $\varphi' > 25^{\circ}$, the growth rate of the resultant force with increasing φ' becomes significantly faster than when $\varphi' \leq 25^{\circ}$. Notably, when φ' exceeds 35°, the resultant force approximately doubles. This necessitates careful consideration in practical design applications.

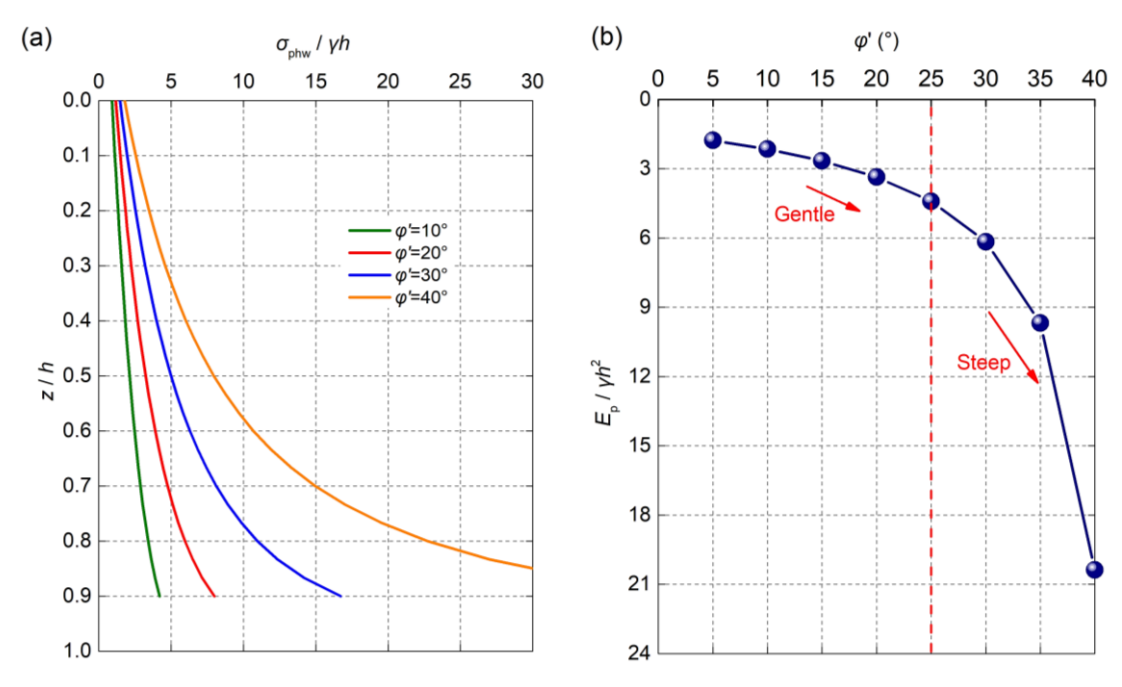


Figure 11. Influence of effective internal friction angle on passive earth pressure: (a) distribution; (b) resultant force

Figure 12 shows the relationship between passive earth pressure and the soil's effective cohesion (c'). The pressure curves for different c' values are nearly parallel. The relationship between the resultant force and c' also exhibits a distinct linear correlation.

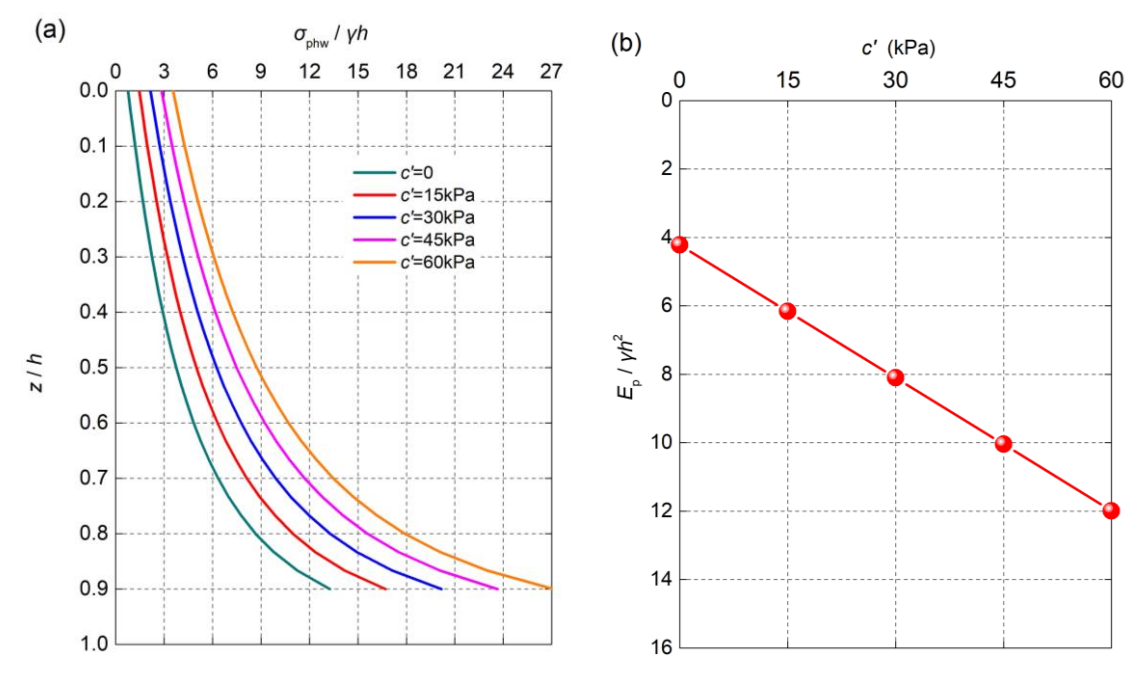


Figure 12. Influence of effective cohesion on passive earth pressure: (a) distribution; (b) resultant force

In summary, the effective friction angle (φ') and the effective cohesion (c') exert the most profound influence on the magnitude of the resultant force. In contrast, the influence of initial matric suction (s_0) , is generally less significant in its absolute magnitude. The groundwater depth (h_w) is highly influential only when shallow, with its effect diminishing rapidly beyond a certain depth.

5.3. Rotation of Principal Stresses

The proposed model explicitly accounts for the rotation of principal stresses, thereby providing a more accurate representation of the actual stress state within the soil behind the wall. The characteristics of this rotation are further depicted in Figure 13. Figure 13-a presents the trajectories of the major principal stress for different δ/φ' ratios, while Figure 13-b illustrates the variation of the angle θ (angle between minor principal stress and horizontal) with δ/φ' . As

 δ/φ' increases, θ increases concomitantly, and the curvature of the major principal stress trajectories becomes more pronounced, indicating greater rotation of principal stresses that exhibits a positive correlation with δ/φ' . Notably, when δ/φ' exceeds 0.8, θ shifts from a linear increase to a sharp decrease. This finding further substantiates the viewpoint presented in Section 5.1 that the proposed model is primarily applicable for $\delta/\varphi' < 0.8$.

The unrealistic surge in passive pressure predicted for $\delta/\varphi' < 0.8$, as shown in Figures 8-b and 13-b signifies a breakdown of the model's underlying assumption of coherent soil arching. Mechanically, this ratio represents a limiting condition where interface friction approaches the soil's internal strength, potentially inducing localized failure rather than global arching. Therefore, the constraint $\delta/\varphi' < 0.8$ is recommended not merely as a numerical limit, but as a general stability criterion for design. This ensures conservative and reliable predictions by preventing over-reliance on interface friction.

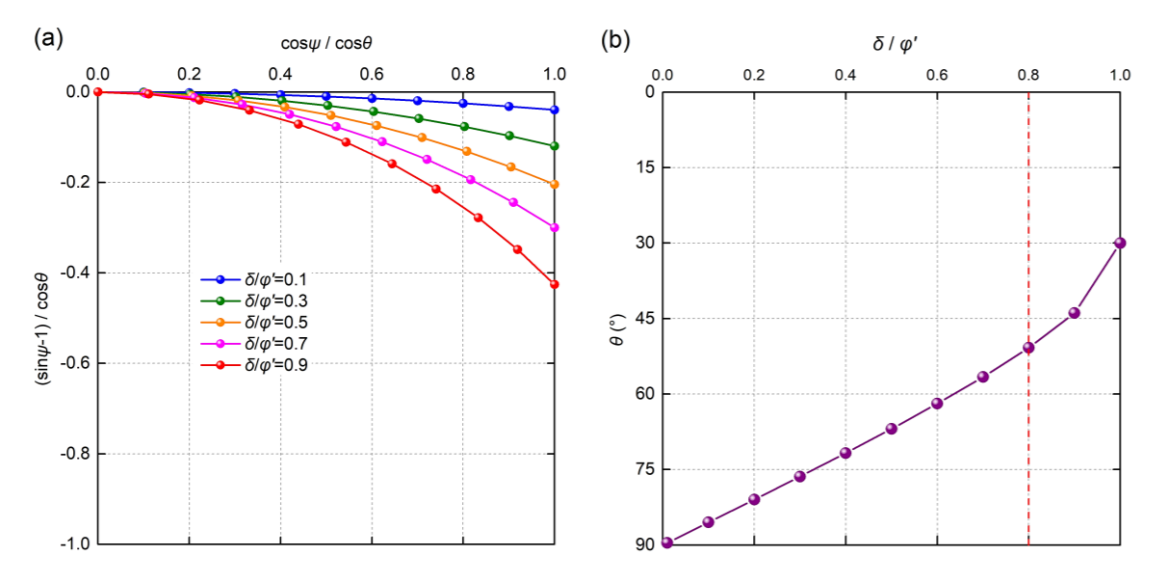


Figure 13. (a) Variation of major principal stress rotation trajectory; (b) Variation of θ at wall-soil interface

The degree of principal stress rotation further governs the magnitudes of the lateral earth pressure coefficient (K_{pw}) and the interlayer shear coefficient (K_{ps}). Figure 14 illustrates the variation of the two coefficients with δ/φ' . As δ/φ' increases, K_{pw} exhibits a gradual decrease, with the rate of reduction accelerating. This indicates that greater wall roughness intensifies principal stress rotation, thereby diminishing the transformation of vertical stress into horizontal earth pressure. Conversely, K_{ps} increases with higher δ/φ' , implying that enhanced wall roughness amplifies interlayer shear interactions within the soil mass and elevates shear stresses.

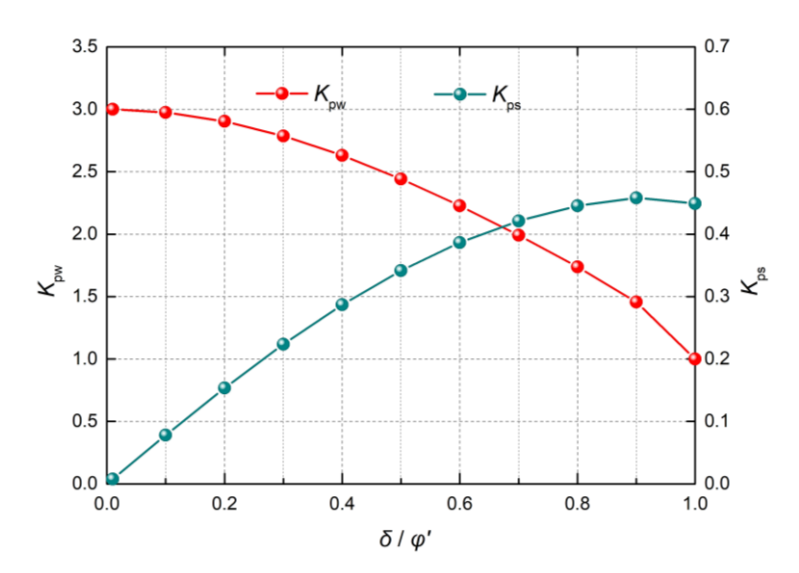


Figure 14. Influence of wall-soil interface friction on K_{pw} and K_{ps}

5.4. Applicability of Key Model Assumptions

The proposed analytical model is built upon two fundamental assumptions: a linear distribution of matric suction under hydrostatic conditions, and a circular-arc trajectory for the rotating major principal stress. The rationale, implications, and generality of these assumptions are discussed herein.

• Assumption of Matric Suction Distribution

The model assumes a hydrostatic pore-water pressure condition, leading to a linear decrease in matric suction from a maximum at the ground surface to zero at the groundwater table (GWT). This represents a significant advancement over models that simplistically assume a constant suction profile, as it more accurately reflects the typical field condition in the absence of infiltration or evaporation [2].

It is important to note that this linear profile is the exact theoretical solution for the steady-state, hydrostatic case. Furthermore, the proposed framework exhibits generality: as the GWT depth approaches infinity, the model naturally reduces to the constant-suction case, demonstrating that the latter is a special case of the former.

While transient hydrological processes (e.g., rainfall infiltration, evaporation) will generate nonlinear suction profiles, the current analytical solution provides a critical baseline for the hydrostatic condition. More importantly, the developed theoretical framework is inherently capable of incorporating more complex hydrology. The variable s(z) in the differential equilibrium equation (Equation 21) can, in principle, be replaced by any function s(z, t) derived from an appropriate seepage analysis. The resulting equation could then be solved numerically, for instance, through an iterative finite-difference scheme. This establishes a clear and valuable pathway for future research to extend the model's applicability to transient seepage scenarios, albeit at the cost of losing a closed-form solution.

• Assumption of Principal Stress Trajectory

The selection of a circular arc to represent the trajectory of the major principal stress is primarily motivated by its mathematical tractability, which is essential for deriving a closed-form analytical solution. This assumption is well-established in the literature concerning earth pressure calculations incorporating arching effects in saturated soils [14, 20, 36].

A pertinent question is whether alternative shapes, such as a catenary or a parabola [30, 31], would yield significantly different results. Comparative studies in the context of saturated soils suggest that the influence of the specific arch shape on the calculated earth pressure magnitude is generally small and can be considered negligible for practical engineering purposes [40]. The fundamental mechanics of stress redistribution due to arching are captured effectively by the circular arc model. Therefore, given its simplicity and demonstrated adequacy, the circular arc assumption represents a robust and justified simplification that enables the derivation of a practical solution without compromising the core physical insights into the coupled effects of soil arching and unsaturated seepage.

6. Conclusions

This study has developed and validated an analytical model for predicting passive earth pressure in unsaturated soils, explicitly accounting for the soil arching effect. The main findings are summarized as follows:

- The incorporation of soil arching reveals a nonlinear distribution of passive earth pressure with depth, contrasting with the linear profile assumed in classical theories. The rotation of principal stresses, influenced by the wall-soil interface friction, significantly alters the stress state within the soil mass.
- The proposed model provides substantially higher estimates of passive earth pressure compared to the extended Rankine theory, which tends to underestimate the resistance in unsaturated backfills. This underscores the importance of considering stress rotation in practical designs.
- Key parameters governing passive earth pressure include the groundwater table depth, initial matric suction, effective friction angle, and effective cohesion. Among these, the effective friction angle has the most pronounced effect, particularly beyond a threshold value of 25°, where the resultant force increases sharply.
- The model is validated through comparisons with experimental data and numerical simulations, showing strong agreement in the upper and middle sections of the wall. However, it is recommended that the model be applied with caution near the wall base (below z/h=0.8) and for high interface friction ratios ($\delta/\phi'>0.8$), where predictions may become unrealistic.
- The analytical framework established herein not only enhances the theoretical understanding of unsaturated soil structure interaction but also provides a practical tool for improving the safety and efficiency of retaining wall design under unsaturated conditions.

7. Declarations

7.1. Author Contributions

Conceptualization, D.J.W. and Q.Y.W.; methodology, D.J.W.; validation, T.W. and Y.H.Z.; formal analysis, D.J.W. and D.J.W.; writing—original draft preparation, D.J.W. and D.J.W.; writing—review and editing, Q.Y.W., T.W., and Y.H.Z.; supervision, Q.Y.W. All authors have read and agreed to the published version of the manuscript.

7.2. Data Availability Statement

The data presented in this study are available on request from the corresponding author.

7.3. Funding

This research was funded by the National Natural Science Foundation of China (NSFC) (Grant No.42307223), Scientific Research Plan of Hubei Provincial Department of Education (Grant No. Q20243001), Scientific Research Foundation of Hubei University of Education for Talent Introduction (Grant No. ESRC20240038), and PowerChina Huadong Engineering Corporation Limited (Grant No. KY2023-JZ-02-13).

7.4. Conflicts of Interest

The authors declare no conflict of interest.

8. References

- [1] Vann, J. D., & Houston, S. L. (2021). Field Soil Suction Profiles for Expansive Soil. Journal of Geotechnical and Geoenvironmental Engineering, 147(9), 4021080. doi:10.1061/(asce)gt.1943-5606.0002570.
- [2] Lu, N., & Griffiths, D. V. (2004). Profiles of Steady-State Suction Stress in Unsaturated Soils. Journal of Geotechnical and Geoenvironmental Engineering, 130(10), 1063–1076. doi:10.1061/(asce)1090-0241(2004)130:10(1063).
- [3] Wang, Z. Y., & Lin, H. (2025). Passive earth pressure of narrow backfill considering seismic-unsaturated seepage multi-field coupling effect. Journal of Central South University, 32(4), 1447–1467. doi:10.1007/s11771-025-5867-9.
- [4] Fredlund, D. G., & Rahardjo, H. (1993). Soil Mechanics for Unsaturated Soils. John Wiley & Sons, Hoboken, United States. doi:10.1002/9780470172759.
- [5] Lu, N., & Likos, W.J. (2004) Unsaturated Soil Mechanics. John Wiley & Sons, Hoboken, United States.
- [6] Vo, T., & Russell, A. R. (2017). Interaction between Retaining Walls and Unsaturated Soils in Experiments and Using Slip Line Theory. Journal of Engineering Mechanics, 143(4), 4016120. doi:10.1061/(asce)em.1943-7889.0001187.
- [7] Deng, B., & Yang, M. (2019). Analysis of Passive Earth Pressure for Unsaturated Retaining Structures. International Journal of Geomechanics, 19(12), 6019016. doi:10.1061/(asce)gm.1943-5622.0001518.
- [8] Zhao, X., Fan, H., & Xu, J. (2024). Stability Analysis for Three-Dimensional Earth-Retaining Structures Subjected to Rainfall Based on a Modified Green–Ampt Model. International Journal of Geomechanics, 24(1), 4023244. doi:10.1061/ijgnai.gmeng-8304.
- [9] Sarkar, S., Shingwekar, E., & Chakraborty, M. (2023). Revisiting Lateral Earth Pressures for Retaining Wall Backfilled with Unsaturated Soil. Geotechnical and Geological Engineering, 41(7), 3985–4006. doi:10.1007/s10706-023-02500-x.
- [10] Fang, W., Cui, Y., & Liu, S. (2025). Nonlinear Rankine pressure of unsaturated soil under transient infiltration. Canadian Geotechnical Journal, 62, 1–16. doi:10.1139/cgj-2024-0408.
- [11] Tracy, F. T., & Vahedifard, F. (2025). Analytical solutions for coupled hydromechanical modeling of lateral earth pressures in unsaturated soils. Computers and Geotechnics, 179, 107038. doi:10.1016/j.compgeo.2024.107038.
- [12] Zhang, Z. L., Zhu, J. Q., & Yang, X. L. (2023). Three-Dimensional Active Earth Pressures for Unsaturated Backfills with Cracks Considering Steady Seepage. International Journal of Geomechanics, 23(2), 4022270. doi:10.1061/(asce)gm.1943-5622.0002648.
- [13] Liu, S., Yuan, Z., Xiao, Y., Fang, Q., & Liu, H. (2025). Profiles of suction stress of layered soils under infiltration conditions and its applications. European Journal of Environmental and Civil Engineering, 29(1), 64-88. doi:10.1080/19648189.2024.2368146.
- [14] Handy, R. L. (1985). The Arch in Soil Arching. Journal of Geotechnical Engineering, 111(3), 302–318. doi:10.1061/(asce)0733-9410(1985)111:3(302).
- [15] Khosravi, M. H., Pipatpongsa, T., & Takemura, J. (2013). Experimental analysis of earth pressure against rigid retaining walls under translation mode. Géotechnique, 63(12), 1020–1028. doi:10.1680/geot.12.p.021.
- [16] Yang, K., Li, Z., Chen, Y., Yang, X., & Lin, W. (2023). Soil Arching–Induced Lateral Earth Pressure Redistribution on the Retaining Wall in a Multistrutted Excavation in Soft Soil. Journal of Geotechnical and Geoenvironmental Engineering, 149(10), 5023004. doi:10.1061/jggefk.gteng-11032.
- [17] Perozzi, D., & Puzrin, A. M. (2024). Experimental Study of the Earth Pressure Evolution on a Model Wall Rotating about Its Base. Journal of Geotechnical and Geoenvironmental Engineering, 150(7), 4024048. doi:10.1061/jggefk.gteng-12163.
- [18] Khosravi, M. H., Bahaaddini, M., Kargar, A. R., & Pipatpongsa, T. (2018). Soil Arching Behind Retaining Walls under Active Translation Mode: Review and New Insights. International Journal of Mining and Geo-Engineering, 52(2), 131–140. doi:10.22059/ijmge.2018.264011.594754.
- [19] Jiang, J., Zhao, Q., Zhu, S., Peng, S., & Wu, Y. (2021). Arching effect and displacement on theoretical estimation for lateral force acting on retaining wall. Natural Hazards, 108(3), 2991–3019. doi:10.1007/s11069-021-04810-w.

[20] Lai, F., Zhang, N., Liu, S., & Yang, D. (2024). A generalised analytical framework for active earth pressure on retaining walls with narrow soil. Géotechnique, 74(11), 1127–1142. doi:10.1680/jgeot.21.00305.

- [21] Deng, B., Long, W., He, Z., & Gao, Y. (2025). Semi-Analytical Solution for Passive Earth Pressure in Unsaturated Narrow Soils Behind Retaining Walls with a Log-Spiral Failure Surface Based on the Principal Stress Trajectory Method. International Journal for Numerical and Analytical Methods in Geomechanics, 49(10), 2432–2454. doi:10.1002/nag.3995.
- [22] Cavalcante, A. L. B., & Zornberg, J. G. (2017). Efficient Approach to Solving Transient Unsaturated Flow Problems. I: Analytical Solutions. International Journal of Geomechanics, 17(7), 04017013. doi:10.1061/(asce)gm.1943-5622.0000875.
- [23] Iiyama, I. (2016). Differences between field-monitored and laboratory-measured soil moisture characteristics. Soil Science and Plant Nutrition, 62(5–6), 416–422. doi:10.1080/00380768.2016.1242367.
- [24] van Genuchten, M. T. (1980). A Closed- form Equation for Predicting the Hydraulic Conductivity of Unsaturated Soils. Soil Science Society of America Journal, 44(5), 892-898. doi:10.2136/sssaj1980.03615995004400050002x.
- [25] Vanapalli, S. K., & Fredlund, D. G. (2000). Comparison of Different Procedures to Predict Unsaturated Soil Shear Strength. Advances in Unsaturated Geotechnics, 195–209. doi:10.1061/40510(287)13.
- [26] Terzaghi, K. (1943). Theoretical Soil Mechanics. John Wiley & Sons, Hoboken, United States. doi:10.1002/9780470172766.
- [27] Iglesia, G. R., Einstein, H. H., & Whitman, R. V. (2014). Investigation of Soil Arching with Centrifuge Tests. Journal of Geotechnical and Geoenvironmental Engineering, 140(2), 4013005. doi:10.1061/(asce)gt.1943-5606.0000998.
- [28] Han, J., Wang, F., Al-Naddaf, M., & Xu, C. (2017). Progressive Development of Two-Dimensional Soil Arching with Displacement. International Journal of Geomechanics, 17(12), 4017112. doi:10.1061/(asce)gm.1943-5622.0001025.
- [29] Tao, F. J., Xu, Y., Zhang, Z., Ye, G. B., Han, J., Cheng, B. N., Liu, L., & Yang, T. L. (2023). Progressive development of soil arching based on multiple-trapdoor tests. Acta Geotechnica, 18(6), 3061–3076. doi:10.1007/s11440-022-01757-5.
- [30] Paik, K. H., & Salgado, R. (2003). Estimation of active earth pressure against rigid retaining walls considering arching effects. Geotechnique, 53(7), 643–653. doi:10.1680/geot.2003.53.7.643.
- [31] Goel, S., & Patra, N. R. (2008). Effect of Arching on Active Earth Pressure for Rigid Retaining Walls Considering Translation Mode. International Journal of Geomechanics, 8(2), 123–133. doi:10.1061/(asce)1532-3641(2008)8:2(123).
- [32] Cong, L., Yang, X. yu, Zhang, B. chang, & Xiong, W. (2022). Estimation of Active Earth Pressure for Limited Width of Soil Using Nonlinear Failure Criterion. Geotechnical and Geological Engineering, 40(9), 4837–4846. doi:10.1007/s10706-022-02187-6.
- [33] Rui, R., Ye, Y., Han, J., Zhang, L., & Zhai, Y. (2020). Experimental and Theoretical Investigations on Active Earth Pressure Distributions behind Rigid Retaining Walls with Narrow Backfill under a Translational Mode. International Journal of Geomechanics, 20(10), 4020178. doi:10.1061/(asce)gm.1943-5622.0001832.
- [34] Li, J. P., & Wang, M. (2014). Simplified Method for Calculating Active Earth Pressure on Rigid Retaining Walls Considering the Arching Effect under Translational Mode. International Journal of Geomechanics, 14(2), 282–290. doi:10.1061/(asce)gm.1943-5622.0000313.
- [35] He, Z. ming, Liu, Z. fu, Liu, X. hong, & Bian, H. bing. (2020). Improved method for determining active earth pressure considering arching effect and actual slip surface. Journal of Central South University, 27(7), 2032–2042. doi:10.1007/s11771-020-4428-5.
- [36] Liu, H., & Kong, D. (2022). Active Earth Pressure of Finite Width Soil Considering Intermediate Principal Stress and Soil Arching Effects. International Journal of Geomechanics, 22(3), 4021294. doi:10.1061/(asce)gm.1943-5622.0002298.
- [37] Cai, Y., Chen, Q., Zhou, Y., Nimbalkar, S., & Yu, J. (2017). Estimation of Passive Earth Pressure against Rigid Retaining Wall Considering Arching Effect in Cohesive-Frictional Backfill under Translation Mode. International Journal of Geomechanics, 17(4), 4016093. doi:10.1061/(asce)gm.1943-5622.0000786.
- [38] Yu, P., Wu, K., Li, D., & Liu, Y. (2025). Passive Earth Pressure and Soil Arch Shape: A Two-Dimensional Analysis. Applied Sciences (Switzerland), 15(11), 6345. doi:10.3390/app15116345.
- [39] Santoso, A. K., & Saito, T. (2024). An Investigation of Dynamic Soil-Structure Interaction on the Seismic Behavior of RC Base-Isolated Buildings. Civil Engineering Journal, 10(11), 3455–3472. doi:10.28991/CEJ-2024-010-11-01.
- [40] Yu, P., & Liu, Y. (2024). Analysis of Active Earth Pressure Behind Rigid Retaining Walls Considering Curved Slip Surface. Geotechnical and Geological Engineering, 42(1), 251–270. doi:10.1007/s10706-023-02567-6.